

Pion single charge exchange on ^{14}C from 35 to 295 MeV

J. L. Ullmann, P. W. F. Alons, J. J. Kraushaar, J. H. Mitchell,
R. J. Peterson, and R. A. Ristinen
Department of Physics, University of Colorado, Boulder, Colorado 80309

J. N. Knudson and J. R. Comfort
Department of Physics, Arizona State University, Tempe, Arizona 85287

H. W. Baer, J. D. Bowman, M. D. Cooper, D. H. Fitzgerald, F. Irom,
M. J. Leitch, and E. Piasezky*
Los Alamos National Laboratory, Los Alamos, New Mexico 87545

(Received 24 June 1985; revised manuscript received 20 February 1986)

The $^{14}\text{C}(\pi^+, \pi^0)^{14}\text{N}$ reaction to the isobaric analog state has been studied at pion energies between 35 and 100 MeV as an extension of earlier measurements at 100 to 295 MeV. Absolute differential cross sections were measured over the 0° – 25° angular range, except at 49.3 MeV, where the range was extended to 75° . A deep minimum was found in the 0° excitation function near 50 MeV, similar to that in the $\pi^-p \rightarrow \pi^0n$ excitation function due to the near cancellation of the S - and P -wave contributions. A comparison of the data with several theoretical models is presented.

I. INTRODUCTION

The nuclear structure of the mass-14 isospin multiplet has made the ^{14}C nucleus a particularly useful target for studying reactions to analog states related by isospin invariance. This target nucleus has been the subject of a series of pion scattering measurements at various beam energies between 35 and 300 MeV. These measurements include the (π^+, π^0) reaction to the isobaric-analog state (IAS), the (π^+, π^-) reaction to the double-isobaric analog state (DIAS), and π^+ and π^- elastic scattering. Preliminary reports on the double-charge-exchange and elastic-scattering measurements at 164 MeV have been made.¹ Two double-charge-exchange (DCX) experiments have been completed at 50 MeV.^{2,3} Single-charge-exchange (SCX) data have been reported previously for energies between 100 and 300 MeV (Ref. 4) and elastic-scattering data at 50 MeV (Ref. 36) and 65 and 80 MeV (Ref. 5) have also been published.

A full report is presented here of measurements of the forward-angle cross sections for the $^{14}\text{C}(\pi^+, \pi^0)$ reaction to the 0^+ IAS at 2.31 MeV in ^{14}N at incident pion energies from 35 to 295 MeV. The 0° cross sections at energies of 100, 165, 230, and 295 MeV were published previously.⁴ The angular range of the measurements is from 0° to approximately 25° . At 49.3 MeV, the range of scattering angles was extended to 75° because of the importance of the single-charge-exchange mechanism to the interpretation of recent 50 MeV DCX data.^{2,3} The larger angular range at 49.3 MeV also permits a comparison between the 0^+ to 0^+ IAS transition of ^{14}C and the $\frac{1}{2}^-$ to $\frac{1}{2}^-$ IAS transition previously measured⁶ for ^{15}N at 48 MeV.

This work represents the first comprehensive study of the IAS cross section over a range of energies from well below the Δ_{33} resonance to above it. Over this energy range, the πN reaction dynamics change considerably from weak and interfering S - and P -wave amplitudes

below 100 MeV, through dominance of the P_{33} amplitude from about 100 to 230 MeV, to a region of slightly weaker interactions at higher energies. Near 45 MeV, the spin-independent isovector S - and P -wave amplitudes nearly cancel, resulting in a dramatic dip in the free πN SCX cross sections at forward angles. In order to evaluate theoretical descriptions that attempt to treat these dynamical changes in a comprehensive manner, a complete data set is needed. Isospin symmetry can be used to relate elastic scattering and single and double charge exchange to the isobaric analog states.

Several quite different theoretical approaches currently exist for calculating π -nucleus scattering over the full range of interest. Studies of elastic scattering near resonance^{7,8} and at lower energies^{9,10} have shown that an optical-model approach provides a good description of the data. Johnson and Siciliano¹¹ have extended the optical potential of Refs. 9 and 10 by adding an explicit isospin dependence so that elastic scattering and SCX and DCX reactions can be described in a coupled-channels framework. Kaufmann and Gibbs¹² calculate charge-exchange scattering in a microscopic three-body model. Recently, the delta-hole model has also been applied¹³ to the SCX and DCX reactions on ^{14}C .

A description of the experimental procedures is given in Sec. II. The empirical results are given in Sec. III along with a general analysis and interpretation. Some detailed comparisons with the Johnson-Siciliano¹¹ and Kaufmann-Gibbs¹² theoretical methods are given in Sec. IV.

II. EXPERIMENTAL METHOD

A. Data acquisition and ^{14}C target

The $^{14}\text{C}(\pi^+, \pi^0)^{14}\text{N}(\text{IAS})$ measurements were carried out with the π^0 spectrometer located in the low-energy pion (LEP) channel at the Clinton P. Anderson Meson

Physics Facility (LAMPF). The π^0 spectrometer detects the two photons emitted in π^0 decay, and has been described in detail elsewhere.¹⁴ The momentum spread, $\Delta P/P$, of the channel ranged from 4% at 35 MeV (yielding a pion beam-energy spread of 2.5 MeV) to 0.7% at 100 MeV (for an energy spread of 1.1 MeV). Typical π^+ fluxes ranged from about 5×10^7 π^+ /sec at 35 MeV to 3×10^8 π^+ /sec at 100 MeV. At 50 MeV the momentum spread was 3% and the average π^+ flux was 2.1×10^7 π^+ /sec. The relative beam flux was measured with respect to the primary proton beam monitor. Absolute flux calibration was provided at each energy by activation measurements of the $^{12}\text{C}(\pi^\pm, \pi\text{N})^{11}\text{C}$ reaction.¹⁵ The pion energy loss in the ^{14}C target ranged from 1.6 MeV at 35 MeV to about 0.8 MeV at 100 MeV.

The target consisted of 9.2 g of powder composed of ^{14}C , ^{12}C , and small amounts of impurities. A recent analysis¹ of the composition of this sample, based on elastic pion scattering at 164 MeV, showed that $9.0 \pm 3.7\%$ of the sample weight consisted of oxygen, magnesium, and aluminum or silicon. The ^{14}C to ^{12}C atomic ratio, 4.6 ± 0.4 , was determined at Oak Ridge National Laboratory by use of mass spectrometry. Thus the actual quantity of ^{14}C contained in the target cells was 7.04 ± 0.31 g. The sample powder was pressed into two 5.0 by 4.9 by 0.6 cm target cells, which were placed back-to-back in the beam. The total ^{14}C thickness was 0.29 ± 0.03 g/cm², where the error includes an estimate for the target nonuniformity. The target cells for the 1982 data runs were made of nickel with each window having a thickness of 0.022 g/cm². For the 1983 and 1984 data runs, the cells were made of copper with each window having a thickness of 0.045 g/cm². The cross sections given in our previous article⁴ must be multiplied by the factor 1.10 to correct for the sample impurities which were subsequently found.¹

Data were taken with the spectrometer set for the $\gamma\text{-}\gamma$ opening angle in the vertical plane (the "one-post" configuration). Three gamma-ray converter planes were used in each arm of the spectrometer. For the 80 and 100 MeV runs, the first converter in each detector arm was set 73 cm from the target with a central opening angle of 75.7 deg. With this setup, the spectrometer acceptance peak was at a π^0 energy of 85 MeV, and the range of π^0 scattering angles with the spectrometer centered at 0° scattering angle was 0°–20°. For the lower energies, the first converters were 55 cm from the target with an opening angle of 92.4 deg. In this configuration, the acceptance was a maximum at a π^0 energy near 50 MeV and the spectrometer acceptance spanned an angular range of 0°–30° in the scattering plane when centered at the 0° location. At 50 MeV, data were taken with the spectrometer central angle set at 0°, 20°, 40°, and 60°.

Data on the $\pi^-p \rightarrow \pi^0n$ reaction were taken at several energies and angles with a CH_2 target as a check on the spectrometer energy scale, efficiency, and instrumental line shape, as discussed below.

B. Software constraints

The total energy of the detected π^0 is related to the laboratory energies (E_1, E_2) and opening angle (η) of its two

decay photons by the relation¹⁴

$$E_{\pi^0}^2 = \frac{2m_{\pi^0}^2 c^4}{(1 - \cos\eta)(1 - X^2)}, \quad (1)$$

where X is the energy-sharing parameter, $X = (E_1 - E_2)/(E_1 + E_2)$. The experimental energy resolution for the π^0 depends on the allowed value for X . For the present data X was constrained to be less than 0.15, which resulted in a calculated energy resolution ranging from 3.5 MeV at a π^0 energy of 35 MeV to 5 MeV at 100 MeV.

An important criterion in the analysis of the data is to ensure that those events whose charged-particle shower is not contained in the lead-glass total-energy calorimeter of the spectrometer are excluded. This is accomplished by requiring that the vertex of a photon conversion in the lead-glass conversion plane preceding the calorimeter lies within the pyramidal volume whose apex is located at the target and whose base is the plane located at a depth $n\chi_0$ within the calorimeter. Here χ_0 is the radiation length (4.35 cm) of the lead glass and n is chosen so as not to affect the resolution or line shape resulting from monoenergetic π^0 s. The value $n = 8$ was used for the $T_\pi \geq 65$ MeV data, while the lower-energy photons arising from the $T_\pi \leq 50$ MeV data were contained for $n = 3$.

The data at each spectrometer angle were typically divided by software into three scattering-angle bins whose widths were chosen so that the yields in each bin would be comparable. To improve statistical accuracy, only two bins were used for the 0° data at 49.3 MeV. Table I lists the approximate ranges of each of the angular bins over which the data were integrated.

C. Spectrometer efficiency and solid angle

The measured cross sections depend on the geometric solid angle and several efficiencies associated with components of the π^0 spectrometer.¹⁴ The multi-wire proportional counter efficiencies, ϵ_{MWPC} , were calculated internally from the data by using the method of Ref. 14. The joint six-chamber efficiencies ranged from 70% to 80% for this experiment. The ray-tracing efficiency, ϵ_f , was taken as $(90 \pm 5\%)$ based on experience with the spectrometer at higher energies. The joint conversion probability, ϵ_{JK} , for both photons to convert into charged particles in the two arms, J and K , of the spectrometer is given by

TABLE I. Angle bins selected for the angular distribution data.

Beam energy (MeV)	Central angle (deg)	Angular ranges (deg)
35	0	0–8, 8–13, 13–30
42.5	0	0–10, 10–18, 18–30
50	0	0–12, 12–24, 24–50
	20	0–16, 16–24, 24–50
	40	10–36, 36–44, 44–70
	60	30–56, 56–64, 64–90
65	0	0–7.5, 7.5–13, 13–30
80	0	0–6, 6–10, 10–30
100	0	0–5.5, 5.5–10, 10–30

$$\epsilon_{JK} = [1 - (1 - \epsilon_C)^3]^2 \quad (2)$$

assuming three identical conversion planes in each arm, a single plane photon conversion probability of ϵ_C , and 100% detection efficiency. For the analysis of the ^{14}C data, values of ϵ_C were taken to be the same for all of the planes and the numerical values were obtained from the following:¹⁴

$$\epsilon_C = 0.86[0.327 + 0.1 \log(0.01E_\gamma)] \quad (3)$$

where E_γ is the photon energy in MeV. The factor 0.86 is due to a reduction in converter thickness to 2.4 cm from the 2.8 cm originally used in formulating the expression.

The geometric solid angle for each angle bin was calculated by a Monte Carlo simulation program¹⁴ and had values of 1–3 msr for the eight-radiation-length gates and 3–6.5 msr for the three-radiation-length gates, depending on angle and energy. Figure 1 shows the spectrometer acceptance calculated by the Monte Carlo program for the low-energy configuration both for the middle angle bin with the spectrometer at 40° (average angle of 40°) and for the forward-angle bin with the spectrometer set at 0° (average angle of 6.5°).

Data were taken on the $\pi^-p \rightarrow \pi^0n$ reaction by using a CH_2 target as a check on the peak shape and solid angle calculated by the Monte Carlo program and on the overall detector efficiency. Figure 2 shows the spectrum obtained from the $\pi^-p \rightarrow \pi^0n$ reaction at 50 MeV and 40° average angle. The calculated peak shape is a very good representation of the data.

Above 100 MeV, different phase-shift predictions of the forward-angle $\pi^-p \rightarrow \pi^0n$ cross sections are in good agreement with the data^{16,17} and can be used to determine the spectrometer solid angle and efficiency. This method was

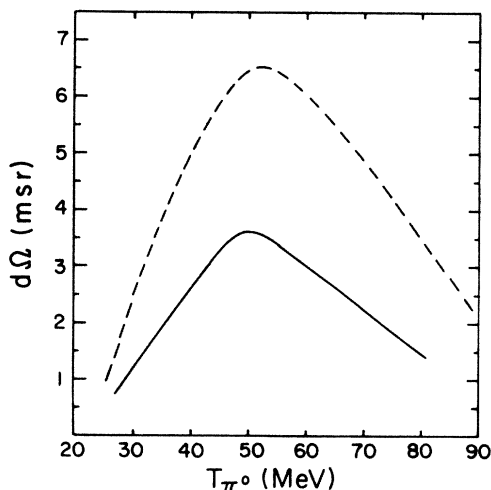


FIG. 1. The spectrometer acceptance calculated by the Monte Carlo program for the low-energy configuration. The solid curve is for an average laboratory angle of 40° and the dashed curve for an average laboratory angle of 6.5° . The solid angle of the latter is larger because of a larger angular acceptance. Both curves are calculated for a three-radiation-length fiducial area and with X , the energy-sharing parameter, constrained to be 0.15 or less.

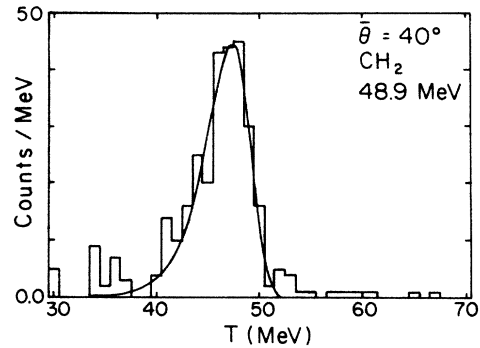


FIG. 2. The π^0 spectrum from the $\pi^-p \rightarrow \pi^0n$ reaction at 48.9 MeV with the spectrometer set for an average laboratory angle of 40° . The solid line is the peak shape calculated with the Monte Carlo program.

used for the ^{14}C data at 100 MeV and above that were previously published.⁴ However, below 100 MeV πN charge exchange data have been scarce and the cross sections change rapidly with energy. Although charge-exchange cross sections near 50 MeV have been measured recently,¹⁸ the data have not yet been included in phase shift analyses. Figure 3 shows the cross sections near 50 MeV calculated from Arndt's FP84 phase shifts,¹⁷ which are based totally on π^\pm elastic scattering. We see that although the cross sections at 0° depend strongly on energy, they are quite stable beyond 40° . The low-energy Karlsruhe phase shift predictions,¹⁶ as given by Arndt's program,¹⁷ are also in good agreement at 48.9 MeV with the FP84 predictions.

In view of the insensitivity to energy, the $\pi^-p \rightarrow \pi^0n$ reaction beyond about 40° (c.m.) provides a good consistency check on the spectrometer efficiency. Figure 3 shows

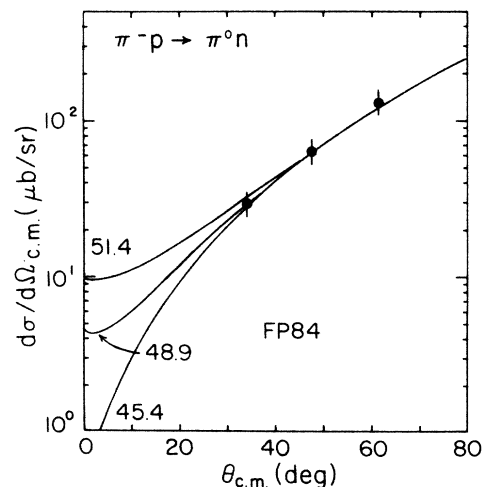


FIG. 3. The 48.9 MeV $\pi^-p \rightarrow \pi^0n$ c.m. cross sections measured in this work. The error bars include all normalization uncertainties. The predictions of Arndt's FP84 phase shifts are also shown for three beam energies.

$\pi^-p \rightarrow \pi^0n$ cross sections at 48.9 MeV determined as described in subsection E. The error bars reflect the 8% uncertainty in the beam flux from the activation cross section¹⁵ as well as all other normalization uncertainties in the efficiencies and solid angle. The agreement with the predictions is excellent, giving us confidence in the normalization procedure. Similar conclusions were made for the data at 65 and 100 MeV.

D. Spectra and yields

Figures 4 and 5 show π^0 energy spectra for the smallest angle bin at several energies. Except at 49.3 MeV, it is seen that the IAS transition to the 2.31 MeV 0^+ state in ^{14}N is the dominant feature of the spectra. Other states near the IAS, such as the unresolvable 1^+ "spin-flip" states at 0 and 3.95 MeV, are not expected to be strongly excited for reasons discussed below. The first level that we expect would be strongly excited above the IAS is the $T=1, 1^-$ state at an excitation energy of 8.06 MeV in ^{14}N . There is evidence for this level in some of the spectra. Figure 6 shows the 49.3 MeV spectrum measured at 60° .

For the 49.3 and 41.8 MeV data, spectra were also measured from a target cell that contained the same amount of ^{12}C as the actual target. These spectra were subtracted

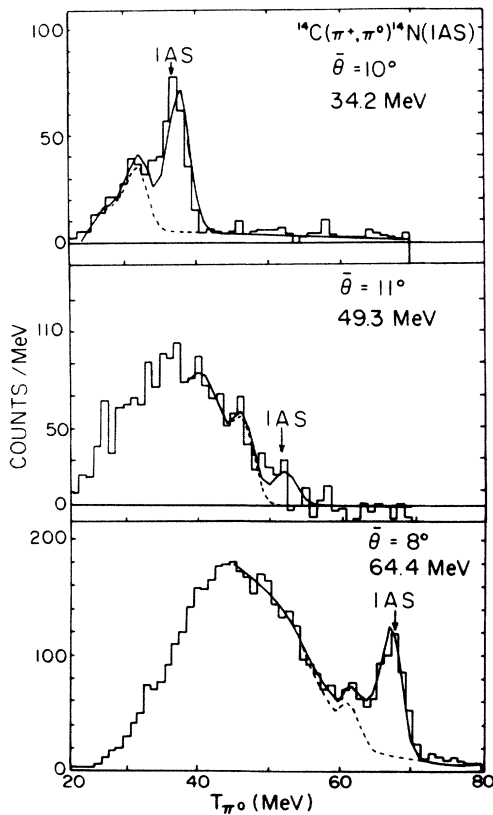


FIG. 4. The π^0 energy spectra for the $^{14}\text{C}(\pi^+, \pi^0)^{14}\text{N}(\text{IAS})$ reaction for the most forward angle bin with the spectrometer set to 0° . The solid line is a fit to the data using the maximum likelihood method described in the text. The dashed line represents the contribution from the background continuum and the 8.06 MeV state in ^{14}N .

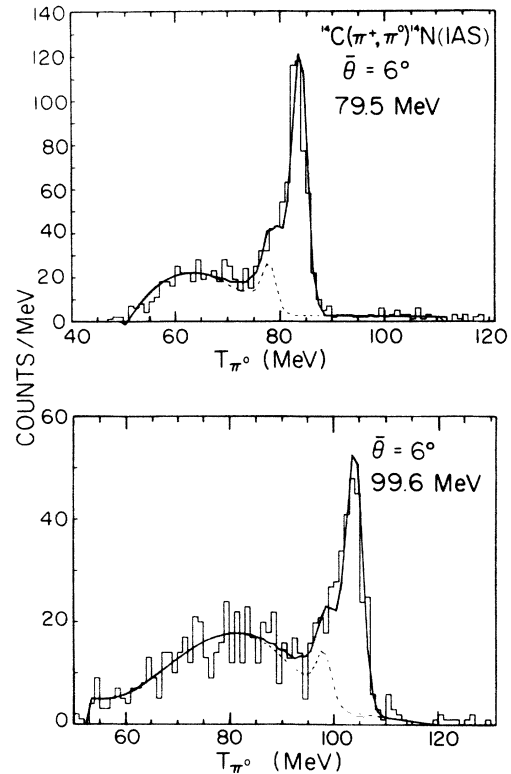


FIG. 5. π^0 spectra, as in Fig. 4, at higher energies.

from the ^{14}C spectra to eliminate events from ^{12}C and the copper cell.

Two methods were used to extract peak areas for the IAS. Both methods took the peak shape from Monte Carlo calculations at each angle and energy. In the first method, a maximum likelihood technique based on Poisson statistics as described by Cooper *et al.*¹⁹ was used. The region of interest was assumed to consist of the IAS peak, a peak at 8.06 MeV excitation, a second- or third-order polynomial to fit the nuclear continuum, plus a linear instrumental background. The results of this fitting procedure are shown as the solid lines in the spectra in Fig. 4. The contribution of the peak at 8.06 MeV,

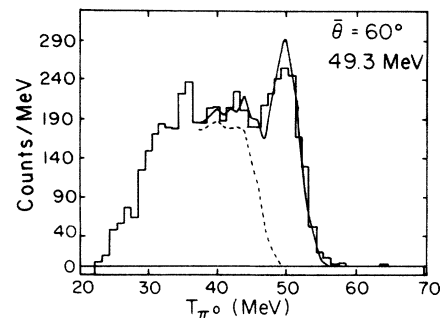


FIG. 6. The π^0 energy spectrum for the $^{14}\text{C}(\pi^+, \pi^0)$ reaction at 49.3 MeV, as in Fig. 4, but at an average laboratory angle of 60° . Any contribution from the 1^+ state at 3.95 MeV could not be separated from the IAS at 2.31 MeV by fitting.

the continuum and the background, is shown as a dashed line in the spectra. The IAS peak area is the difference between the solid and dashed lines.

The second method used a least-squares technique based on Gaussian statistics and an analytic representation of the Monte Carlo peak shape. In this method the nuclear continuum and background were assumed to be represented by two straight lines with the continuum beginning at the peak centroid. The main difference in the methods was in the shape assumed for the nuclear continuum.

The results of the two methods were typically consistent within statistical accuracy. In the few cases where the areas were not consistent, the uncertainties were increased to reflect the difference. The final cross sections were based on peak areas from the first method.

Because of the very small cross sections at 49.3 MeV, a careful evaluation of the uncertainties in the fitting procedure was carried out at that energy. Varying the assumed peak location ± 1 MeV from its kinematic location resulted in a 10% variation in the peak area for angle bins at both the 0° and 60° spectrometer locations. A comparison of the two peak extraction methods showed that the results obtained with the first method ranged from being 23% higher at 10.5° to 27% lower at 12.6° than those obtained with the second method, these extremes occurring in spectra with poor statistical accuracy. Averaged over all angles, the first method yielded 5% more counts than the second method.

A more serious uncertainty arises because the IAS at 2.31 MeV in ^{14}N cannot be resolved from the 1^+ ground state or the 1^+ state at 3.95 MeV. The latter is dominant in intermediate energy (p,n) studies²⁰ and contains a large fraction of the Gamow-Teller sum rule strength. We must therefore carefully evaluate its contribution to our data, especially at 49.3 MeV, where the non-spin-flip amplitude to the IAS is very small.

Spin-flip cross sections for pions at forward angles are normally expected to be quite small. Based on parity conservation, the cross section is vanishingly small for spin-0 particles at 0° .²¹ Under the adiabatic condition that the Q value is small compared to the beam energy, the unnatural-parity 1^+ cross sections vanish at all angles.²² If the adiabatic condition is not met precisely for a reaction dominated by strong absorption, differential cross sections can be shown to be proportional to $|J_1(kR\theta)|^2$, where k is the incident momentum, R is the effective interaction radius, and θ is the scattering angle. This behavior has been observed for pion scattering to 1^+ states of ^{12}C at beam energies near the (3,3) resonance.²³ Distorted-wave impulse-approximation calculations²⁴ of spin excitation confirm this behavior. Thus, near resonance the forward-angle contribution from the 1^+ states is expected to be small.

Near 50 MeV, the pion is not strongly absorbed, but calculations²⁵ still predict an approximate $|J_1|^2$ behavior for the 0^+ to 1^+ transition, with a peak near 50° . This shape is similar to that for the IAS. We have attempted to estimate the contribution from the 1^+ state in two different ways. First, we added a peak at 3.95 MeV in the fitting procedure for the data near 50° . The results of this

addition implied that $(25 \pm 25)\%$ of the counts could be due to the extra state. This analysis could not be done at forward angles because of poor statistics, and extrapolation to these angles is highly model dependent.

A second estimate of the strength of the transition to the 3.95 MeV state is provided by a preliminary calculation of Gibbs and Siegel.²⁵ They estimate the peak cross section to be about $30 \mu\text{b}$ at 50° . This is about 30% of the measured value.

While there are good indications that some of the cross section may be due the 3.95 MeV state, there are no experimental measurements of inelastic scattering at nearby energies that would enable us to estimate this contribution with certainty. We have therefore elected to report the cross sections by assuming a single state, so that the meaning of the associated statistical and experimental uncertainties is clear.

E. Cross sections

Cross sections were calculated from the following relationship:

$$\frac{d\sigma}{d\Omega} = \frac{Y}{\Phi\tau} \frac{\cos\theta_t}{N_t} e^{2\mu_d t_d} e^{\mu_t t_t} \frac{1}{\Delta\Omega_{MC}\epsilon_f\epsilon_{JK}\epsilon_{MWPC}}, \quad (4)$$

where Y is the extracted peak area, Φ is the time-integrated beam flux, τ is the computer lifetime, θ_t is the target angle, and N_t is the number of target nuclei per cm^2 . Attenuation of the decay photons in each detector crate is corrected for in the $e^{2\mu_d t_d}$ term where t_d is the thickness of the CH_2 range attenuator and μ_d is the attenuation coefficient. Photon attenuation in the target is corrected for similarly, where μ_t is the target attenuation and t_t the target thickness. The last term contains efficiencies and the Monte-Carlo (MC) geometric solid angle, $\Delta\Omega_{MC}$. The cross sections are listed in Table II.

The uncertainties in the listed cross sections include both statistical and fitting uncertainties. The overall normalization uncertainty includes contributions of 1% from ϵ_{JK} , 5% from ϵ_f , 15% from ϵ_{MWPC} , 1% from the absorption corrections, 8% from the target thickness, 5% from the Monte Carlo solid angle, and 5% to 8% from the ^{11}C -activation beam flux determination. The total normalization uncertainty thus was about 20% at each energy.

Cross sections at energies of 99.5–294.6 MeV were measured in the 1982 data runs and the 0° cross sections were previously reported.⁴ The values given in Table II have been corrected for the change in target thickness as discussed in Sec. II A. The 99.5 MeV cross sections measured in 1982 and 1983 differ by about 15%. This is within the quoted absolute normalization uncertainty. The target powder was repacked between the two runs, which could explain a major portion of the discrepancy.

III. EXPERIMENTAL RESULTS AND ANALYSIS

The angular distributions measured at average pion energies of 34.2, 41.8, 49.3, 64.4, and 79.5 MeV at the center of the target are shown in Fig. 7. These energies correspond to beam energies of 35, 42.5, 50, 65, and 80 MeV.

TABLE II. Center of mass cross sections for the $^{14}\text{C}(\pi^+, \pi^0)^{14}\text{N}(\text{IAS})$ reaction. T_π is the π^+ laboratory energy at the center of the target.

T_π (MeV)	$\theta_{\text{c.m.}}$ (deg)	$d\sigma/d\Omega_{\text{c.m.}}$ ($\mu\text{b}/\text{sr}$)
34.2	9.8	61 ± 4
	13.0	66 ± 5
	20.0	65 ± 3
41.8	10.1	17.5 ± 5.5
	15.4	40.6 ± 4.8
	23.2	41.1 ± 10.4
49.3	10.6	9.7 ± 3.8
	12.8	12.0 ± 1.9
	18.5	12.3 ± 4.2
	18.5	19.0 ± 8.0
	21.7	24.4 ± 2.6
	29.9	36.0 ± 6.6
	34.0	62.0 ± 3.2
	41.5	86.2 ± 8.8
	49.8	97.1 ± 7.3
	54.0	130.0 ± 8.0
	61.9	134.0 ± 8.0
74.4	138.0 ± 8.0	
64.4	7.8	152 ± 16
	12.0	136 ± 14
	18.9	100 ± 14
79.5	6.6	581 ± 26
	9.5	549 ± 24
	14.2	407 ± 19
99.6	5.8	986 ± 71
	8.9	959 ± 60
	14.7	791 ± 57
99.5	5.3	1390 ± 100
	7.7	1170 ± 70
	11.0	1160 ± 70
	16.0	980 ± 70
164.5	4.2	2460 ± 170
	7.0	2160 ± 130
	10.3	1610 ± 130
	16.2	1240 ± 150
229.5	3.7	2650 ± 190
	6.3	1860 ± 160
	8.8	1820 ± 180
	13.1	1030 ± 150
294.6	3.3	1870 ± 150
	6.1	1570 ± 170
	8.9	1210 ± 200
	12.8	590 ± 220

Those measured at 99.5, 164.5, 229.5, and 294.6 MeV, corresponding to beam energies of 100, 165, 230, and 295 MeV, are shown in Fig. 8. The error bars reflect only statistical and peak-fitting uncertainties. The curves are the results of calculations that will be discussed in Sec. IV.

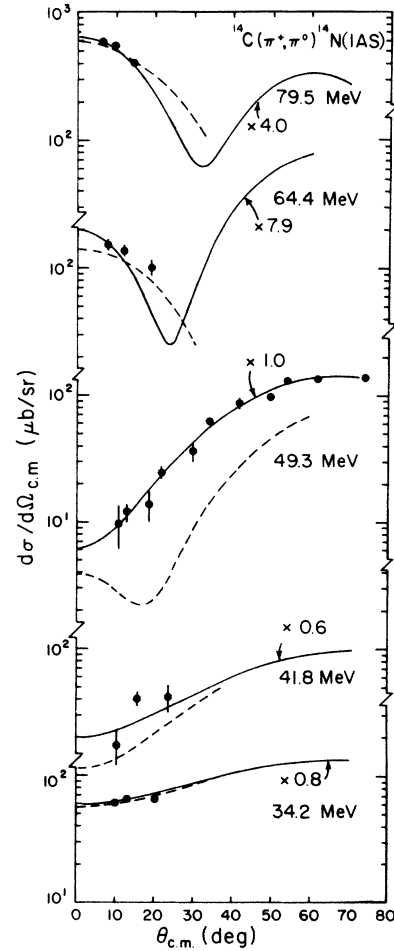


FIG. 7. π^0 angular distributions at energies below 80 MeV. Error bars do not include the normalization uncertainty at each energy. The points and errors assume a single state, and are not corrected for any possible contribution from unresolved nearby states. The dashed curves are the results of unrenormalized plane-wave calculations. The solid curves, renormalized by the factors shown at each energy, are the results of optical-model calculations with a parameter determined by fitting the 49.3 MeV data, as described in the text.

The angular distributions at the higher energies are forward peaked as expected for diffractive scattering. The low-energy angular distributions shown in Fig. 7 qualitatively reflect the strongly energy-dependent nature of the free πN charge exchange cross section. A dramatic forward-angle dip in the data at 49.3 MeV is seen due to the near cancellation of the isovector non-spin-flip S - and P -wave amplitudes. This interference does not occur in the isoscalar or isovector spin-dependent component of the interaction. In view of the recent interest in the $^{14}\text{C}(\pi^+, \pi^-)(\text{DIAS})$ reaction at 50 MeV, we measured a more complete angular distribution for the IAS transition at that energy.

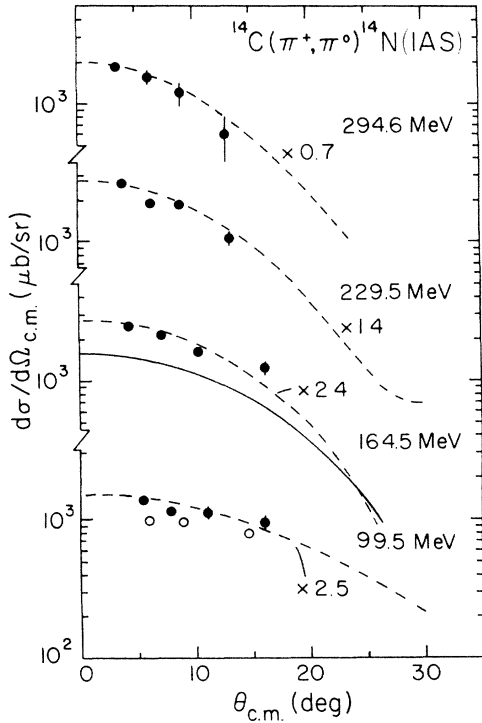


FIG. 8. π^0 angular distributions above 80 MeV. The error bars do not include the normalization uncertainty at each energy. The open circles were measured in 1983, the solid dots in 1982. The dashed lines, renormalized by the factors shown for each energy, are the results of first-order optical model calculations described in the text. The unrenormalized solid line at 164.5 MeV is the result of a second-order calculation.

A. $d\sigma/d\Omega(0^\circ)$ as a function of energy

In order to estimate the 0° cross sections, the angular distributions at each energy except 49.3 MeV were fitted by the function

$$\frac{d\sigma(\theta)}{d\Omega} = A - Bq^2(\theta), \quad (5)$$

where q is the c.m. momentum transfer. This form represents a small-angle approximation to a Legendre polynomial expansion. The 0° extrapolation at 49.3 MeV is discussed in Sec. III B. The values of the 0° cross sections are given in Table III and shown in Figs. 9 and 10. The uncertainties shown include uncertainties from the extrapolation as well as the normalization uncertainties of the original data. The values at 100 MeV and above differ from those previously reported⁴ because of the target thickness correction discussed in Sec. II and a different 0° extrapolation procedure.

The solid lines in Figs. 9 and 10 are the 0° free $\pi^+n \rightarrow \pi^0p$ cross sections calculated from Arndt's recent FP84 phase shifts.¹⁷ These cross sections are plotted in the laboratory frame to approximate the π -nucleus kinematics and have been multiplied by two because there are two excess neutrons in ^{14}C . One can see that the π -

TABLE III. The 0° c.m. cross sections for the $^{14}\text{C}(\pi^+, \pi^0)^{14}\text{N}(\text{IAS})$ reaction. T_π is the laboratory energy at the center of the target.

T_π (MeV)	$(d\sigma/d\Omega_{\text{c.m.}})_0$ ($\mu\text{b/sr}$)
34.2	62 ± 12
41.8	18 ± 6
49.3	6 ± 3
64.4	160 ± 30
79.5	640 ± 130
99.6	1160 ± 240
164.5	2350 ± 370
229.5	2470 ± 400
294.6	1920 ± 320

nucleus data follow the general trend of the free cross sections, although they appear to be shifted to higher energy.

The energy at which the minimum of the measured 0° excitation function occurs was estimated by fitting a fourth-order polynomial to the data between 35 and 100 MeV, as shown in Fig. 9. The minimum of this curve is at 48.3 MeV. Fits with lower-order polynomials or with the inclusion of the 164 MeV data point yield minima within 2 MeV of this value. Thus, we estimate the minimum of the 0° cross section to occur at 48 ± 2 MeV. This value is shifted from the calculated minimum of the free πN cross section at 44.3 MeV, but is consistent with the Coulomb-corrected energy of the minimum observed in other nuclei.²⁶

B. 50 MeV data

At 49.3 MeV, two extrapolated quantities, the 0° cross section and the angle-integrated cross section, have been determined. To do this, the data at 49.3 MeV were fitted with the function

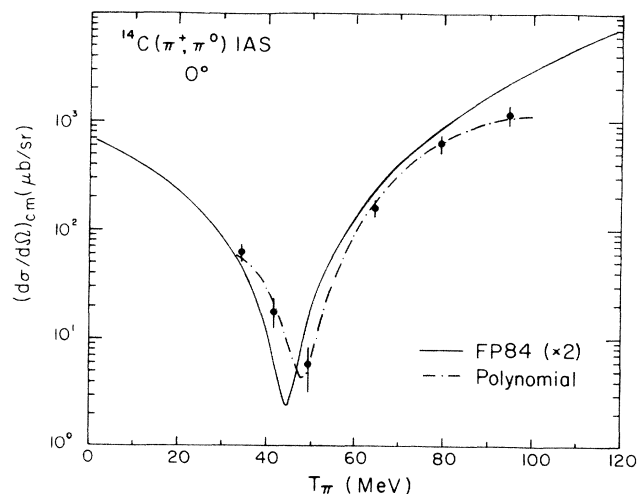


FIG. 9. The 0° c.m. cross section plotted vs laboratory energy for the $^{14}\text{C}(\pi^+, \pi^0)\text{IAS}$ reaction. The error bars include normalization uncertainties. FP84 is the free $\pi^+n \rightarrow \pi^0p$ cross section, multiplied by 2, calculated from Arndt's FP84 phase shifts (Ref. 17). The dash-dot curve is the result of a fourth-order polynomial fit to the data.

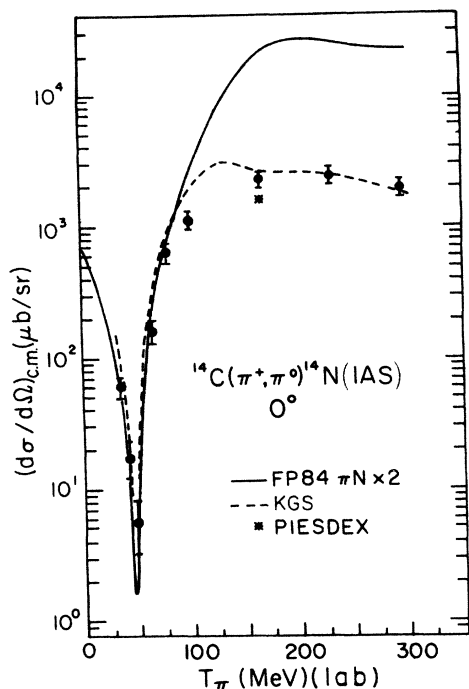


FIG. 10. The 0° c.m. cross sections plotted versus laboratory energy over the full energy range. The error bars include normalization uncertainties. FP84 is the free $\pi^+n \rightarrow \pi^0p$ cross section (Ref. 17) multiplied by 2, and KGS indicates the calculation of Kaufmann, Gibbs, and Siegel (Ref. 12). The points labeled PIESEDEX are the results of second-order PIESEDEX calculations at the two energies where a full parameter set has been determined.

$$\frac{d\sigma}{d\Omega} = \left| \sum_{l=0}^3 (2l+1) a_l P_l(\cos\theta) \right|^2, \quad (6)$$

were the a_l are complex coefficients and the P_l are Legendre polynomials. This function gives an excellent fit to the data, as illustrated in Fig. 11. The 0° cross section obtained with this fit is $7 \pm 1 \mu\text{b/sr}$. Other fits, which did not include some of the large-angle data points, gave 0° values ranging from 3 to $8 \mu\text{b/sr}$. The extrapolation to 0° is a sensitive function of the order of the polynomial expansion and the number of data points included in the fit. In view of all the uncertainties involved, we assign to the 0° cross section a value of $6 \pm 3 \mu\text{b/sr}$.

The differential cross sections of the continuum integrated between 14 and 24 MeV excitation in the residual ^{14}N nucleus are also shown in Fig. 11. These cross sections also rise with angle, but more slowly than the IAS, again reflecting the backward peaking of the free πN cross section. The angle-integrated cross section from 0° to 90° for this 10 MeV interval, determined by using the function shown with the data, is 0.17 mb. Extending the integral to 180° results in a cross section of 0.5 mb.

To estimate the angle-integrated cross section for the IAS, the shape of the $^{15}\text{N}(\pi^+, \pi^0)(\text{IAS})$ angular distribution⁶ was used for the large-angle points. To do this, the ^{15}N data were normalized to the ^{14}C data at 50° . The re-

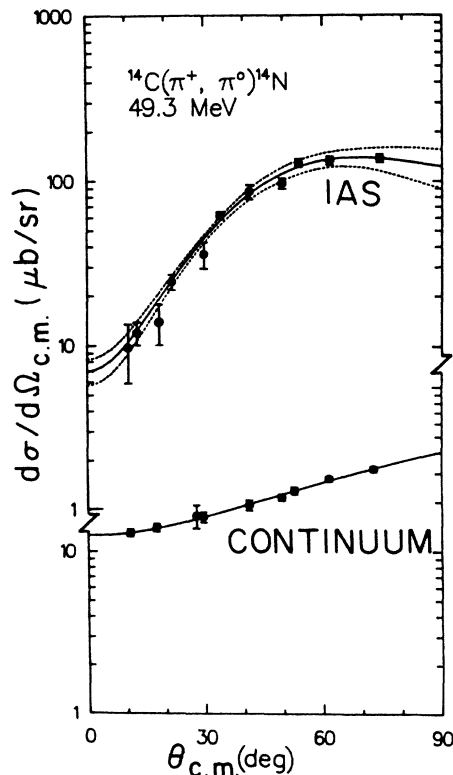


FIG. 11. The cross section to the IAS compared to a region of the continuum at 49.3 MeV. The solid curves are the results of polynomial fits to the data, and the dashed lines are the region of uncertainty of the fit.

sulting composite angular distribution is shown in Fig. 12. The combined data were then fitted with the Legendre expansion of Eq. (6), leading to the curve shown in Fig. 12. The integral of this function out to 90° is 0.67 ± 0.02 mb, and the integral to 180° is 1.32 ± 0.07 mb. To estimate the error in the 75° – 180° contribution, maximum and minimum plausible lines were drawn between 180° and the last data point at 75° . These lines yielded values for the angle-integrated cross section of 1.72 and 1.11 mb, which lead to an uncertainty of 0.3 mb in the model-dependent value. The adopted value for the angle-integrated cross section is then 1.32 ± 0.30 mb, not including the uncertainty in the possible contribution from the 1^+ state.

This result can be compared to the value of 0.43 ± 0.07 mb for the IAS transition in ^{15}N at 48 MeV,⁶ also measured with the π^0 spectrometer, and with the value of 0.67 ± 0.07 mb for the IAS transition in ^{13}C ,²⁷ determined by radio-chemical methods. Thus one can see that $\sigma_{\text{IAS}}(^{14}\text{C}) \simeq 2\sigma_{\text{IAS}}(^{13}\text{C})$ and $\sigma_{\text{IAS}}(^{14}\text{C}) \simeq 3\sigma_{\text{IAS}}(^{15}\text{N})$.

The ^{14}C data at 49.3 MeV are compared directly to the ^{15}N data⁶ measured earlier at 48.0 MeV in Fig. 13. The shapes of the two angular distributions seem to be quite similar over the common angular range. The ratio of differential cross sections, $^{14}\text{C}/^{15}\text{N}$, at 50° is 2.9 ± 0.7 . This large value of the ratio is somewhat surprising, since one

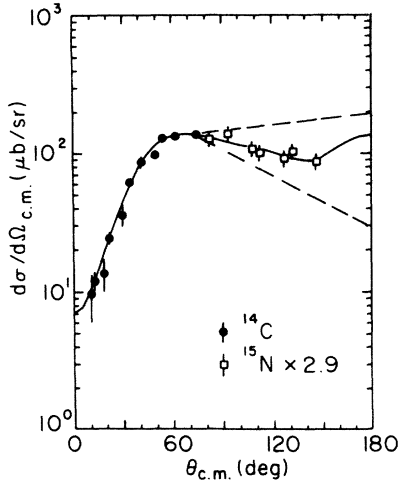


FIG. 12. Extrapolation of the $^{14}\text{C}(\pi^+, \pi^0)$ data at 49.3 MeV to 180° , as discussed in the text. The solid line is a polynomial fit to the data, and the dashed lines represent the limits of plausible extrapolation.

might expect some $\Delta S=1$ contribution to the ^{15}N cross section, producing a ratio of less than two. However, analysis of ^{15}O beta decay²⁸ implies that the $\Delta S=1$ contribution is less than 10% of the $\Delta S=0$ portion. The fact that the observed ratio is larger than what is expected may reflect an inadequate understanding of nuclear structure of the two nuclei or a rapid energy dependence of the medium corrections, but may also indicate a contribution to the ^{14}C cross section from the 1^+ state.

IV. THEORETICAL DESCRIPTIONS

Several theoretical approaches to the pion-nucleus interaction are currently under development by various

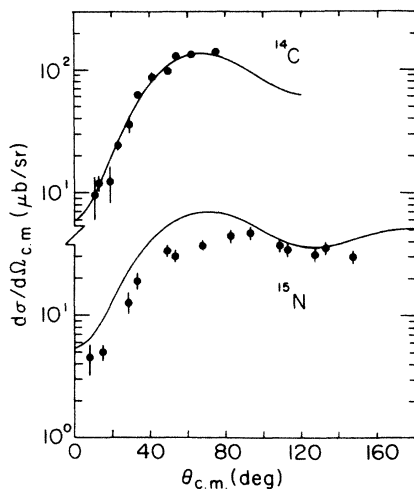


FIG. 13. The ^{14}C data at 49.3 MeV from this work compared to $^{15}\text{N}(\pi^+, \pi^0)$ IAS data at 48 MeV from Ref. 6. The solid curves are optical model calculations with the same second-order parameters, shown in Table IV. Error bars do not include normalization uncertainties, and the points assume a single state.

groups. We will first discuss a simple plane wave calculation which describes the 50 MeV data well. Next we will compare the data either to published calculations, or calculations that we have made based on published descriptions of the reaction mechanism.

Two models relevant to the data presented here have been published by Johnson and Siciliano^{11,29} and by Kaufmann and Gibbs.¹² Although there is undoubtedly considerable overlap in the physics that has been assumed and incorporated in these treatments, the approach and language of each model is quite distinct. Both methods generate optical potentials by starting with the pion-nucleon phase shifts, but the manner in which nuclear binding effects are included is quite different. The accurate treatment of these effects appears to be crucial to the description of the SCX reaction. We emphasize that because the dynamics of the πN interaction change rapidly near 45 MeV, it is essential for any calculation to use phase shifts that adequately describe the free πN scattering. The calculations presented here will either use phase shifts²⁵ based on recent $\pi^-p \rightarrow \pi^0n$ data¹⁸ or Arndt's FP84 phase shifts¹⁷ which are reasonably consistent with Ref. 18.

A. Plane wave calculations

The simplest approach to calculating the angular distributions is to assume plane-wave scattering. The dashed lines in Fig. 7 are the unrenormalized results of plane-wave calculations made with the PIESDEX code³⁰ and the FP84 phase shifts¹⁷ with an excess-neutron transition density to be discussed later. The energy at which the phase shifts were evaluated was shifted down by 5 MeV from the kinematic value. This shift was motivated by the difference in energy between the minimum in the 0° excitation function of the free πN process and the ^{14}C excitation function. Figure 7 shows that the agreement with the data is excellent, except at 49.3 MeV. This simple description of the data is probably due to the energy shift simulating medium effects that were needed to describe elastic scattering in this energy range.^{5,9,10}

To aid the understanding of the forward-angle scattering, analytic plane-wave Born-approximation calculations were performed by using the approximate expression.

$$\frac{d\sigma}{d\Omega} = (N - Z) \frac{k^2}{k_c^2} |f_S + f_P \cos\theta|^2 \times \left| 4\pi \int_0^\infty \frac{\sin qr}{qr} \rho(r) r^2 dr \right|^2. \quad (7)$$

Here f_S and f_P are the free S - and P -wave scattering amplitudes which form the non-spin-flip amplitude, ρ is the ground state excess neutron density, q and k are the momentum transfer and pion momentum in the π -nucleus c.m. system, and k_c is the pion momentum in the π -nucleon c.m. system. The amplitudes f_S and f_P are evaluated in the π -nucleon c.m. system and are functions of k_c . The density $\rho(r)$ is normalized to unity.

In general the results of these calculations are very similar to those of the PIESDEX plane-wave calculations shown in Fig. 7. At 64.4 and 79.5 MeV, the angular dis-

tributions are forward peaked. Since f_P is larger than f_S at these energies, it follows from Eq. (7) that this forward peaking is due to the term $f_P^2 \cos^2 \theta$ in the cross section. Below 41.8 MeV, the S -wave amplitudes become larger than the P -wave amplitudes and the forward peaking disappears.

Near 45 MeV, the free S - and P -wave amplitudes are of equal magnitude but of opposite sign, providing an extremely sensitive region for studying the modification of the πN amplitudes in the nuclear medium. This feature is illustrated by the results at 49.3 MeV. The solid curve in Fig. 14 is the result of a calculation at 49.3 MeV based on Eq. (7). In this calculation we used the πN amplitudes determined from fits²⁵ to the forward-angle $\pi^-p \rightarrow \pi^0n$ data of Fitzgerald *et al.*,¹⁸ and a P -shell harmonic oscillator density for $\rho(r)$ with an oscillator parameter of 1.74 fm (corresponding to an rms radius of 2.56 fm). The result of this calculation shows a dip in the cross section near 30° which is not present in the data. If the oscillator parameter is decreased to 1.63 fm, the cross section at 0° is unchanged and at 90° increases from 180 to 230 $\mu\text{b}/\text{sr}$, but the dip near 25° remains. Multiplying the P -wave term by a factor of 0.9 eliminates the dip, and provides a better overall representation of the shape of the angular distribution, as seen in Fig. 14. A similar result is obtained by enhancing the S -wave amplitude by a factor of 1.1, as also shown in Fig. 14. These curves are evidence for the modification of P -wave strength relative to S -wave strength in complex nuclei.

A further indication of this modification of the relative S - and P -wave strengths is seen in the 0° excitation function shown in Fig. 9. The energy of the minimum for ^{14}C is 48 ± 2 MeV, compared to the values of 46 MeV for the free $\pi^-p \rightarrow \pi^0n$ process determined by the fits of Siegel and Gibbs,²⁵ or 44.3 MeV from the FP84 phase shifts.¹⁷ Reducing the P -wave amplitude of Siegel and Gibbs by 10% shifts the minimum in the plane-wave calculation from 46 to 49 MeV, in qualitative agreement with the ^{14}C data.

Both the shape of the angular distribution at 49.3 MeV and the 0° excitation function are consistent (in the plane wave model) with a modification of the isovector P -wave strength relative to the isovector S -wave strength, similar to what was observed previously in the isoscalar channel.^{9,10} This may be due to Coulomb distortions,²⁵ a Lorentz-Lorenz type of effect, off-shell behavior of the πN amplitudes in the nuclear medium, nuclear binding energy effects, or a combination of these.

B. Johnson-Siciliano method

The approach of Johnson and Siciliano¹¹ is a microscopic optical-model description of the π -nucleus interaction that was originally proposed for energies in the Δ region and has recently been extended to lower energies.²⁹ The model assumes that the isobaric analog states and ground state are degenerate members of an isospin multiplet and that scattering between them can be simply related by isospin symmetry. Terms in the optical potential that are of first-order in the nuclear density are determined by the free π -nucleon t matrix, with corrections for

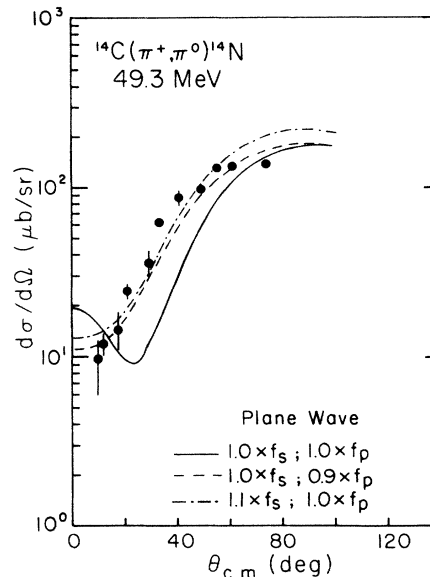


FIG. 14. Plane wave calculations for $^{14}\text{C}(\pi^+, \pi^0)\text{IAS}$ at 49.3 MeV. The solid curve used isovector S - and P -wave amplitudes determined from a fit to π -nucleon data, while the dashed curve is the result of a calculation with the P -wave amplitudes reduced by 10%. Enhancing the S -wave amplitude by 10% yields the dot-dash curve.

Pauli-blocking and long-range Pauli correlations included below 100 MeV. Terms of second-order or higher in the nuclear density that are associated with long- and short-range correlations and true absorption are included with adjustable coefficients.

We made our calculations by using Siciliano's code PIESEX.³⁰ Arndt's FP84 phase shifts¹⁷ were used to calculate the π -nucleon interaction. An excess-neutron density ($\Delta\rho$) was used in calculating the IAS transition as suggested by Auerbach *et al.*³¹ Both $\Delta\rho$ and the ground state density were derived from a Hartree-Fock calculation using the Skyrme-III force.³²

At low energies, the Johnson-Siciliano potential reduces to the Michigan State University (MSU) potential of Refs. 9 and 10 when the isotensor terms are set to zero and the isovector terms are written explicitly for π^+ and π^- scattering. At 50 MeV, π^\pm - ^{14}C elastic scattering³⁶ is well described by the MSU potential and the parameters tabulated in Refs. 9 and 10. Although not shown, explicit PIESEX calculations, with isoscalar second-order parameters from set C, Table IV of Ref. 10, also reproduce the elastic data. We have included Pauli-blocking effects in the PIESEX calculations below 100 MeV by multiplying the imaginary part of the first-order terms by a "Pauli factor" as suggested by Landau and McMillan.³³

The second-order portion of the Johnson-Siciliano potential can be thought of as requiring six complex empirical parameters: two each (S - and P -wave) in the isoscalar, isovector, and isotensor channels. At 50 MeV, the isoscalar parameters can be taken from Ref. 10. Siciliano^{6,29} has then shown that the isotensor parameters have little effect

TABLE IV. Parameters used in the PIESDEX calculations.

T_π (MeV)	34.2	41.8	49.3	64.4	79.5
$\text{Re}\lambda_0^{(2)}$	-0.162	-0.130	-0.108	-0.080	-0.062
$\text{Im}\lambda_0^{(2)}$	1.133	0.909	0.756	0.558	0.436
$\text{Re}\lambda_0^{(2)}$	0.671	0.669	0.667	0.663	0.659
$\text{Im}\lambda_0^{(2)}$	1.100	1.097	1.093	1.087	1.080
$\text{Im}\lambda_1^{(2)}$	-2.0	-2.0	-2.0	-2.0	-2.0
λ_{LLEE}	1.6	1.6	1.6	1.6	1.6
Pauli factor	0.21	0.26	0.30	0.38	0.44
$\text{Im } b_0$	0.0027	0.0039	0.0052	0.0082	0.0114
$\text{Im } c_0$	0.0095	0.0167	0.0260	0.0553	0.0994

on single charge exchange, and that only the imaginary part of the isovector P -wave parameter need be nonzero to give a good description of the data. We have adjusted this parameter to fit our 49.3 MeV data. The resulting calculations are shown in Fig. 7 as the solid curves. The parameters used in our calculations are given in Table IV. This fit illustrates that optical-model calculations with one free parameter can fit the SCX data at 49.3 MeV.

The second-order parameters of the potential are expected to be energy dependent. Indeed, calculations of π - ^{14}C elastic scattering at 65 and 80 MeV, with the 50 MeV parameters, do not fit the data well. Preliminary studies of an energy-dependent parameter set have been made.³⁴ We investigate here the need for energy-dependent parameters in the SCX channel by doing PIESDEX calculations at other energies below 100 MeV with the parameters determined at 49.3 MeV. We include a rudimentary energy dependence in the Pauli factor and in the kinematical relationship of the Johnson-Siciliano parameters to the MSU parameters. The parameters are shown in Table IV and the calculations as the solid curves in Fig. 7. The calculations must be renormalized by the factors shown in the figure, and clearly do not fit the data away from 49.3 MeV.

These results confirm the energy-dependent nature of the second-order parameters, and suggest that a careful energy-dependent analysis of elastic scattering and single and double charge exchange below 100 MeV is needed.

Comparisons of the PIESDEX calculations with the data at 100 MeV and above are shown in Fig. 8. The dashed lines are the results of calculations made with only the first-order density terms and no Pauli corrections. Those calculations must be renormalized by the factors shown in the figure. The solid line in Fig. 8 is the unrenormalized result of a calculation at 165 MeV done with the second-order parameters determined empirically by Greene *et al.*⁸ Although the results of Ref. 8 are based on the older πN phase shifts of Ref. 35, changing to the FP84 phase shifts makes little difference at 165 MeV. This calculation is in better agreement with the data but is still too low in magnitude. This discrepancy was also observed for other light nuclei⁸ and may indicate some inadequacies in the surface behavior of the Skyrme-III densities for light nuclei, although other explanations are not ruled out. At 294.6 MeV the discrepancy between the calculation and the data may be due in part to the fact that PIESDEX

does not include D -wave or higher-order phase shifts, which are becoming important at these energies.

C. Kaufmann-Gibbs method

The work of Kaufmann and Gibbs¹² provides a microscopic treatment of pion-nucleus scattering and charge-exchange reactions within the framework of a three-body model. The incident pion interacts with a nucleon in the nuclear medium in accordance with the πN interaction described by a potential. This nucleon interacts with the rest of the nucleus, expressed by a spectrum of intermediate states through which it may be scattered. Since the intermediate states corresponding to the ground state are occupied, blocking corrections must be made in the construction of the nonlocal pion-nucleus potential.

Calculations¹² with this method predict that the 0° excitation function for π -nucleus SCX reactions should have a deep minimum near 50 MeV due to the high transparency of the nucleus that is characteristic of this approach. Comparisons with the 0° excitation function for the free $\pi^-p \rightarrow \pi^0n$ reaction (or simple plane-wave calculations) indicate that the pattern given by the model closely resembles that of the free πN process over most of the energy range from 20 to 300 MeV. This feature was emphasized in the earlier work on ^{14}C in the higher energy region.⁴ It arises principally from a large reduction in the absorptive content of the optical potential due to blocking and is most important at lower energies.

The dashed line in Fig. 10 is the result of calculations for ^{14}C made with the full model of Kaufman, Gibbs, and Siegel (KGS).¹² The FP84 set of phase shifts¹⁷ was used in these calculations. The transition operator involves a separable form of the free t matrix and microscopic Woods-Saxon descriptions of the bound neutron-hole and proton-particle states. The results of these calculations differ from results shown in Ref. 4 due to recent extensions and refinements of the model. The calculations give a very reasonable description of the data, especially around the minimum near 50 MeV as well as above 200 MeV.

The calculations shown in Fig. 10 do not include effects of a relative D -wave interaction. It is estimated that such an interaction would increase the 165 MeV cross sections by about 5% and the 295 MeV cross sections by about 25%. Such changes would remain consistent with the data.

V. SUMMARY AND CONCLUSIONS

Angular distributions have been presented for the $^{14}\text{C}(\pi^+, \pi^0)^{14}\text{N}(\text{IAS})$ reaction at energies from 34.2 to 294.6 MeV, spanning the region of the Δ_{33} resonance. The most distinctive feature of these data is a change of the angular distributions from a forward-peaked diffractive shape above 100 MeV, characteristic of black-disk scattering, to a deep forward angle minimum at 49.3 MeV. This behavior reflects the energy dependence of the elementary $\pi^+n \rightarrow \pi^0p$ process, in which the P -wave dominance near 165 MeV changes to an almost perfect cancellation between the isovector S - and P -wave non-spin-flip amplitudes at 49.3 MeV. This cancellation is also obvious in the 0° excitation function, which below 100 MeV follows almost exactly the free π -N values.

The exact energy of the minimum in the 0° excitation function and the shape of the angular distributions near this minimum are very sensitive to the relative strengths of the S - and P -wave amplitudes. The energy of the 0° minimum in $^{14}\text{C}(\pi^+, \pi^0)$ appears to be shifted up in energy relative to the free πN value, showing that the relative S - and P -wave strengths have changed in the nuclear medium. The results of plane-wave calculations in this energy region indicate that the shift may be due to a

modification in complex nuclei of the isovector P -wave strength relative to the isovector S -wave strength. A similar effect has been observed in the isoscalar channel in studies of π -nucleus elastic scattering.^{9,10}

The data have been compared to the calculated results of two distinct theoretical models of the reaction mechanism. The calculation of Kaufmann, Gibbs, and Siegel¹² provides a very good description of the 0° excitation function over the entire energy range. We have also presented the results of calculations using the program PIESEX, based on the coupled-channels optical model of Johnson and Siciliano.¹¹ The calculations used second-order parameters determined only at 49.3 and 165 MeV. As a consequence, only the data at these energies were well described, and a striking energy dependence in this optical-model formulation needs to be investigated.

ACKNOWLEDGMENTS

We wish to thank E.R. Siciliano, P.B. Siegel, W. Kaufman, W. Gibbs, and M.B. Johnson for many helpful discussions on theoretical topics. We are indebted to T. Cunningham for extensive help in the analysis of the data. This work was supported in part by the U.S. Department of Energy and the National Science Foundation.

*Present address: Department of Physics, Tel-Aviv University, Ramat-Aviv, Israel.

¹H. Baer *et al.*, Los Alamos National Laboratory Report No. LA-10070-PR, 1983 (unpublished); C. J. Harvey, H. W. Baer, J. A. Johnstone, C. L. Morris, S. J. Seestrom-Morris, D. Dehnhard, D. B. Holtkamp, and S. J. Green, *Phys. Rev. C* **33**, 1454 (1985).

²I. Navon, M. J. Leitch, D. A. Bryman, T. Numano, P. Schlatter, G. Azuelos, R. Poutissou, R. A. Burnham, M. Hasinoff, J. M. Poutissou, J. A. Macdonald, J. E. Spuller, C. K. Hargrove, H. Mes, M. Blecher, K. Gotow, M. Moinester, and H. Baer, *Phys. Rev. Lett.* **52**, 105 (1984).

³M. J. Leitch, E. Piasetzky, H. W. Baer, J. D. Bowman, R. L. Burman, B. J. Dropesky, P. A. M. Gram, F. Irom, D. Roberts, G. A. Rebka, J. N. Knudson, J. R. Comfort, V. A. Pinnick, D. H. Wright, and S. A. Wood, *Phys. Rev. Lett.* **54**, 1482 (1985).

⁴F. Irom, J. R. Comfort, R. Jeppesen, J. J. Kraushaar, R. A. Ristinen, W. Tew, J. L. Ullmann, H. W. Baer, J. D. Bowman, M. D. Cooper, E. Piasetzky, U. Sennhauser, A. Erell, M. A. Moinester, and E. R. Siciliano, *Phys. Rev. C* **28**, 2565 (1983).

⁵M. Blecher, K. Gotow, R. L. Burman, M. V. Hynes, M. J. Leitch, N. S. Chant, L. Rees, P. G. Roos, F. E. Bertrand, E. E. Gross, F. E. Obenshain, T. P. Sjoreen, G. S. Blanpied, B. M. Freedom, and B. G. Ritchie, *Phys. Rev. C* **28**, 2033 (1983).

⁶M. D. Cooper, H. W. Baer, R. Bolton, J. D. Bowman, F. Cverna, N. S. P. King, M. J. Leitch, J. Alster, A. Doron, A. Erell, M. A. Moinester, E. Blackmore, and E. R. Siciliano, *Phys. Rev. Lett.* **52**, 1100 (1984).

⁷W. B. Cottingham and D. B. Holtkamp, *Phys. Rev. Lett.* **45**, 1828 (1980).

⁸S. J. Greene, C. J. Harvey, P. A. Seidl, R. Gilman, E. R. Siciliano,

and M. B. Johnson, *Phys. Rev. C* **30**, 2003 (1984).

⁹K. Stricker, H. McManus, and J. A. Carr, *Phys. Rev. C* **19**, 929 (1979).

¹⁰K. Stricker, J. A. Carr, and H. McManus, *Phys. Rev. C* **22**, 2043 (1980).

¹¹M. B. Johnson and E. R. Siciliano, *Phys. Rev. C* **27**, 730 (1983); **27**, 1647 (1983).

¹²W. B. Kaufmann and W. R. Gibbs, *Phys. Rev. C* **28**, 1286 (1983); P. B. Siegel and W. B. Kaufman, private communication.

¹³T. Karapiperis and M. Kobayashi, *Phys. Rev. Lett.* **54**, 1230 (1985).

¹⁴H. W. Baer, R. D. Bolton, J. D. Bowman, M. D. Cooper, F. H. Cverna, R. H. Heffner, C. M. Hoffman, N. S. P. King, J. Piffaretti, J. Alster, A. Doron, S. Giland, M. A. Moinester, P. R. Bevington, and E. Winkelmann, *Nucl. Instrum. Methods* **180**, 445 (1981).

¹⁵G. W. Butler, B. J. Dropesky, C. J. Orth, R. E. L. Green, R. J. Korteling, and G. K. Y. Lam, *Phys. Rev. C* **26**, 1737 (1982).

¹⁶G. Höhler, *Pion-Nucleon Scattering: Phenomenological Analyses*, Landolt-Börnstein 962 (Springer, Berlin, 1983), Vol. I.

¹⁷R. A. Arndt, Program SAID (scattering analysis interactive dialin), Virginia Polytechnic Institute and State University, 1984.

¹⁸D. H. Fitzgerald, H. W. Baer, J. D. Bowman, F. Irom, N. S. P. King, M. J. Leitch, E. Piasetzky, W. J. Briscoe, M. E. Sadler, K. Smith, and J. N. Knudson, Los Alamos National Laboratory Report No. LA-UR-86-821, 1986; *Bull. Am. Phys. Soc.* **29**, 676 (1984).

¹⁹M. D. Cooper, H. W. Baer, J. D. Bowman, F. H. Cverna, R. H. Heffner, C. M. Hoffman, N. S. P. King, J. Piffaretti, J. Alster, A. Doron, S. Gilad, M. A. Moinester, P. R. Bevington,

- and E. Winklemann, *Phys. Rev. C* **25**, 438 (1982).
- ²⁰T. N. Taddeucci, T. A. Carey, C. Gaarde, J. Larsen, C. D. Goodman, D. J. Horen, T. Masterson, J. Rapaport, T. P. Welch, and E. Sugarbaker, *Phys. Rev. Lett.* **52**, 1960 (1984).
- ²¹G. Morpurgo, *Phys. Rev.* **131**, 2205 (1963).
- ²²K. Alder and A. Winther, *Nucl. Phys.* **37**, 194 (1962).
- ²³R. J. Peterson, R. L. Boudrie, J. J. Kraushaar, R. A. Ristinen, J. R. Shepard, G. R. Smith, C. F. Moore, W. J. Braithwaite, N. S. P. King, C. L. Morris, H. A. Thiessen, and J. Piffaretti, *Phys. Rev. C* **21**, 1030 (1980).
- ²⁴E. R. Siciliano and G. E. Walker, *Phys. Rev. C* **23**, 2661 (1981).
- ²⁵P. B. Siegel and W. R. Gibbs, private communication.
- ²⁶F. Irom, M. J. Leitch, H. W. Baer, J. D. Bowman, M. D. Cooper, B. J. Dropesky, E. Piazetsky, and J. N. Knudson, *Phys. Rev. Lett.* **55**, 1862 (1985).
- ²⁷D. J. Viera *et al.*, Los Alamos National Laboratory Report LA-9381-P12, 1981 (unpublished).
- ²⁸K. Sugimoto, *Phys. Rev.* **182**, 1051 (1969).
- ²⁹E. R. Siciliano, Proceedings of the LAMPF Workshop on Double Charge Exchange, 1985, Los Alamos National Laboratory Report LA-10550-C, 1985; E. R. Siciliano, M. D. Cooper, M. B. Johnson, and M. J. Leitch (unpublished).
- ³⁰E. R. Siciliano, private communication.
- ³¹N. Auerbach, M. B. Johnson, A. Klein and E. Siciliano, *Phys. Rev. C* **29**, 526 (1984).
- ³²M. Beiner, H. Flocard, Nguyen Van Giai, and P. Quentin, *Nucl. Phys.* **A238**, 29 (1975).
- ³³R. H. Landau and M. McMillan, *Phys. Rev. C* **8**, 2094 (1973).
- ³⁴P. W. F. Alons, J. L. Ullmann, and E. R. Siciliano, *Bull. Am. Phys. Soc.* **30**, 794 (1985).
- ³⁵G. Rowe, M. Salomon, and R. H. Landau, *Phys. Rev. C* **18**, 584 (1978).
- ³⁶C. S. Mishra, B. M. Preedon, B. G. Ritchie, R. S. Moore, M. Blecher, K. Gotow, R. L. Burman, M. U. Hynes, E. Piazetsky, N. S. Chant, P. G. Roos, F. E. Bertrand, T. Sjoreen, F. E. Obenshain, and E. E. Gross, *Phys. Rev. C* **32**, 995 (1985).